

## Giant Pressure Dependence and Dimensionality Switching in a Metal-Organic Quantum Antiferromagnet

B. Wehinger,<sup>1,2,\*</sup> C. Fiolka,<sup>3</sup> A. Lanza,<sup>3</sup> R. Scatena,<sup>3</sup> M. Kubus,<sup>3</sup> A. Grockowiak,<sup>4</sup> W. A. Coniglio,<sup>4</sup> D. Graf,<sup>4</sup> M. Skoulatos,<sup>5</sup> J.-H. Chen,<sup>6,7</sup> J. Gukelberger,<sup>7,8,†</sup> N. Casati,<sup>9</sup> O. Zaharko,<sup>2</sup> P. Macchi,<sup>3</sup> K. W. Krämer,<sup>3</sup> S. Tozer,<sup>4</sup> C. Mudry,<sup>6</sup> B. Normand,<sup>10</sup> and Ch. Rüegg<sup>1,10</sup>

<sup>1</sup>*Department of Quantum Matter Physics, University of Geneva, 24, Quai Ernest Ansermet, CH-1211 Genève, Switzerland*

<sup>2</sup>*Laboratory for Neutron Scattering and Imaging, Paul Scherrer Institute, CH-5232 Villigen-PSI, Switzerland*

<sup>3</sup>*Department of Chemistry and Biochemistry, University of Bern, Freiestrasse 3, CH-3012 Bern, Switzerland*

<sup>4</sup>*National High Magnetic Field Laboratory, 1800 East Paul Dirac Drive, Tallahassee, Florida 32310, USA*

<sup>5</sup>*Heinz-Maier-Leibnitz Zentrum and Physics Department, Technische Universität München, Lichtenbergstrasse 1, 85748 Garching, Germany*

<sup>6</sup>*Condensed Matter Theory Group, Paul Scherrer Institute, CH-5232 Villigen-PSI, Switzerland*

<sup>7</sup>*Theoretical Physics, ETH Zürich, CH-8093 Zürich, Switzerland*

<sup>8</sup>*Département de Physique and Institut Quantique, Université de Sherbrooke, Sherbrooke, Québec, J1K 2R1, Canada*

<sup>9</sup>*Swiss Light Source, Paul Scherrer Institute, CH-5232 Villigen-PSI, Switzerland*

<sup>10</sup>*Neutrons and Muons Research Division, Paul Scherrer Institute, CH-5232 Villigen-PSI, Switzerland*



(Received 8 February 2018; published 11 September 2018)

We report an extraordinary pressure dependence of the magnetic interactions in the metal-organic system  $[\text{CuF}_2(\text{H}_2\text{O})_2]_2\text{pyrazine}$ . At zero pressure, this material realizes a quasi-two-dimensional spin-1/2 square-lattice Heisenberg antiferromagnet. By high-pressure, high-field susceptibility measurements we show that the dominant exchange parameter is reduced continuously by a factor of 2 on compression. Above 18 kbar, a phase transition occurs, inducing an orbital re-ordering that switches the dimensionality, transforming the quasi-two-dimensional lattice into weakly coupled chains. We explain the microscopic mechanisms for both phenomena by combining detailed x-ray and neutron diffraction studies with quantitative modeling using spin-polarized density functional theory.

DOI: [10.1103/PhysRevLett.121.117201](https://doi.org/10.1103/PhysRevLett.121.117201)

Quantum fluctuations are especially strong in low-dimensional systems, giving rise to numerous exotic phenomena in quantum magnetism [1–3]. The design and control of materials with quasi-one-dimensional (Q1D) and quasi-two-dimensional (Q2D) antiferromagnetic (AFM) interactions is of particular interest for potential applications in AFM spintronics, where energy efficiencies are outstanding compared to ferromagnets and the spin dynamics is faster by orders of magnitude [4–6]. A full exploitation of this potential requires further progress in theoretical, experimental, and materials physics, specifically designer low-dimensional materials with experimentally controlled magnetic exchange to benchmark accurate theoretical descriptions.

Metal-organic compounds based on  $\text{Cu}^{2+}$  ions make excellent model quantum magnets because of their localized spin-1/2 moments and large charge gap. Suitable materials are based on soft coordination polymers with rigid linkers such as pyrazine (pyz), which provide  $\text{Cu}^{2+}$  networks with exchange parameters on the scale of 0.1–10 K that are robust and strongly anisotropic in space [7,8]. These interactions can be determined to high accuracy from thermodynamic and spectroscopic

measurements, and interaction control can be achieved by chemistry or physics. Chemical variation of ligands and counterions allows for significant modification [9,10], to the point of dimensionality control [11], while fine-tuning is possible by isotopic substitution [12]. Physically, an applied pressure provides direct control of structural and, in turn, magnetic properties [13,14].

In this Letter, we report on two types of extreme behavior in  $[\text{CuF}_2(\text{H}_2\text{O})_2]_2\text{pyz}$  under pressure. Magnetic susceptibility measurements show massive and continuous changes of the dominant exchange parameters in two different low-dimensional magnetic states. These states, a Q2D spin-1/2 square-lattice antiferromagnet at pressures up to 18 kbar and Q1D AFM chains at higher pressures, are separated by a phase transition which switches the magnetic orbital and thus the dimensionality. By diffraction studies and quantitative modeling using spin-polarized density functional theory (DFT), we show that its origin lies in the pressure sensitivity of superexchange paths involving water ligands. Our results allow unprecedented control of magnetic interactions and thus represent an important step towards materials choices for quantum magnetism by design.

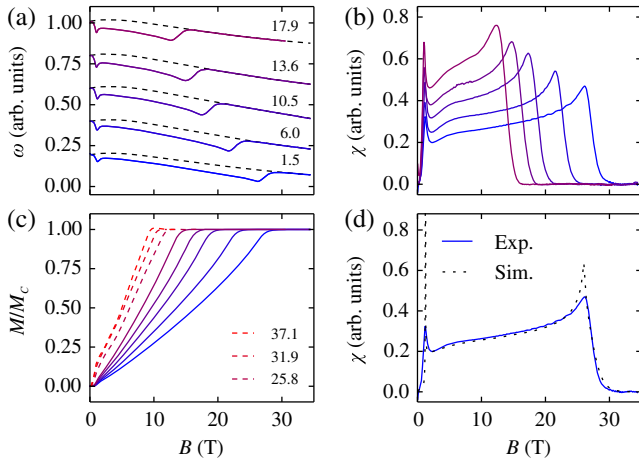


FIG. 1. (a) Measured TDO resonance frequencies  $\omega$  at selected pressures  $P$  (kbar) for  $T = 1.5$  K (solid lines), shown with the magnetoresistive background of the resonator coil (dashed). (b)  $\chi(B)$  for the same  $T$  and  $P$  values. (c)  $M/M_c(B)$  at  $P = 37.1, 31.9,$  and  $25.8$  kbar (dashed lines), measured at  $0.4$  K, and at the pressures shown in panels (a) and (b) (full lines), measured at  $1.5$  K. (d)  $\chi(B)$  at  $1.5$  kbar and  $1.5$  K as obtained from experiment (full line) and from QMC simulations (dashed line).

Single crystals of  $[\text{CuF}_2(\text{H}_2\text{O})_2]_2\text{pyz}$  were grown as described in Sec. S1 of the Supplemental Material (SM) [15]. Magnetic susceptibility measurements were performed using a tunnel diode oscillator (TDO), as detailed in Sec. S2 of the SM [15], while the magnetic exchange was controlled by isotropic compression of a sample aligned with the crystallographic  $a$  axis parallel to the field. We performed two independent experiments using (i) a piston cylinder cell for pressures up to  $17.9$  kbar in fields up to  $35$  T and temperatures down to  $1.5$  K and (ii) a specially designed moissanite anvil cell for pressures up to  $37.1$  kbar with maximum field  $18$  T and minimum temperature  $0.4$  K.

The TDO resonance frequency  $\omega$  is shown in Fig. 1(a) as a function of field at five different pressures and a constant temperature of  $1.5$  K. The magnetic susceptibility,  $\chi = \partial M / \partial B$  in Fig. 1(b), was obtained by subtracting the magnetoresistive background of the resonator coil from  $\omega$ . The peak observed at low fields is due to a spin-flop transition, which occurs at  $B_{\text{sf}} = 1.2$  T at  $1.5$  kbar and shifts to  $1.0$  T at  $17.9$  kbar, then from  $0.84$  T at  $25.8$  kbar to  $0.7$  T at  $37.1$  kbar. Otherwise  $\chi(B)$  shows a gradual increase with field and a pronounced peak prior to saturation. The magnetization,  $M$  [Fig. 1(c)], obtained by integrating  $\chi(B)$ , changes little for fields below  $B_{\text{sf}}$ , then shows increasing field alignment up to a saturation field  $B_c$  that changes dramatically with pressure.

The Néel temperature,  $T_N$  in Fig. 2(a), was determined by measuring the temperature dependence of  $\omega$  at the field  $B = B_{\text{sf}}$  corresponding to each pressure point. This allows for a precise measurement because the changes are particularly pronounced at  $T_N$  (Sec. S2 of the SM [15]). The relative change of  $T_N$  with pressure is also dramatic, and its

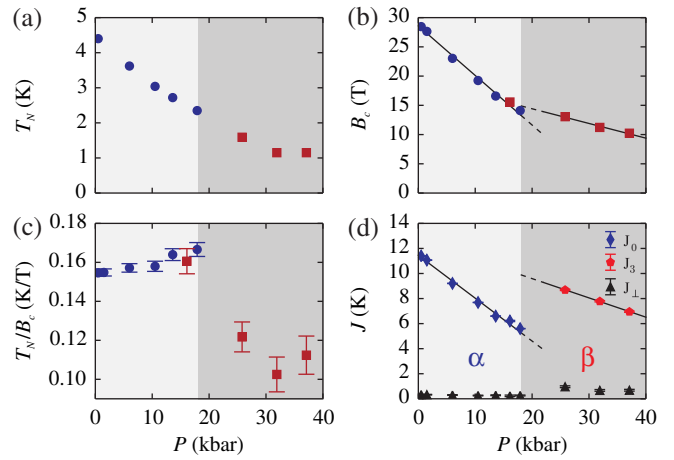


FIG. 2. (a)  $T_N$  measured as a function of  $P$  at field values corresponding to  $B_{\text{sf}}$ . (b)  $B_c$  obtained from self-consistent fitting procedure; black lines show linear fits. Blue circles show data obtained using the piston cell, red squares using the moissanite cell. (c) Ratio  $T_N/B_c$  as a function of  $P$ , illustrating the evolution of dimensionality; the sharp drop marks the phase transition to the Q1D magnetic system. Two missing values of  $T_N$  for calculating  $T_N/B_c$  were obtained from linear interpolation based on panel (a). (d) Exchange parameters obtained from QMC fits to the experimental data, shown together with a linear fit (black lines).

continuous change over such a wide pressure range is quite unprecedented. Because  $T_N$  is a significant fraction of our measurement temperature, care is required to extract the underlying magnetic exchange parameters and we adopt the consistent fitting procedure described next.

At low pressures,  $[\text{CuF}_2(\text{H}_2\text{O})_2]_2\text{pyz}$  is a prototypical spin-1/2 square-lattice antiferromagnet with dominant in-plane magnetic exchange  $J_0$  and weak interlayer interactions [14]. We observe that  $[\text{CuF}_2(\text{H}_2\text{O})_2]_2\text{pyz}$  has three interlayer exchange parameters and analyze  $J_1, J_2,$  and  $J_3$  in connection with Fig. 3, but to complete the experimental analysis we combine them as follows. We have performed neutron diffraction measurements of the magnetic structure of  $[\text{CuF}_2(\text{H}_2\text{O})_2]_2\text{pyz}$ , detailed in Sec. S3 of the SM [15], which establish that the interbilayer coupling  $J_1$  is AFM while the effective intrabilayer coupling  $\tilde{J}_2$ , which is a combination of  $J_2$  and  $J_3$ , is effectively FM. Within the mean-field random-phase-approximation (RPA) treatment [32] summarized in Sec. S5 of the SM [15], one may show that only the sum  $|J_1| + |\tilde{J}_2| = 2J_\perp$  enters the susceptibility, and hence extract a single effective interlayer exchange parameter  $J_\perp$ .

For a full investigation of pressure dependence, we note that  $g\mu_B B_c(P) = 4J_0(P) + 2J_\perp(P)$  is the sum of all interaction strengths at a single  $\text{Cu}^{2+}$  site, with  $g = 2.42$  determined experimentally for  $B \parallel a$  [14].  $J_0(P)$  and  $T_N(P)$  can be used to determine one interlayer exchange parameter by employing the empirical relation

$$J_\perp(P) = J_0(P)e^{b-4\pi\rho_s/T_N(P)}, \quad (1)$$

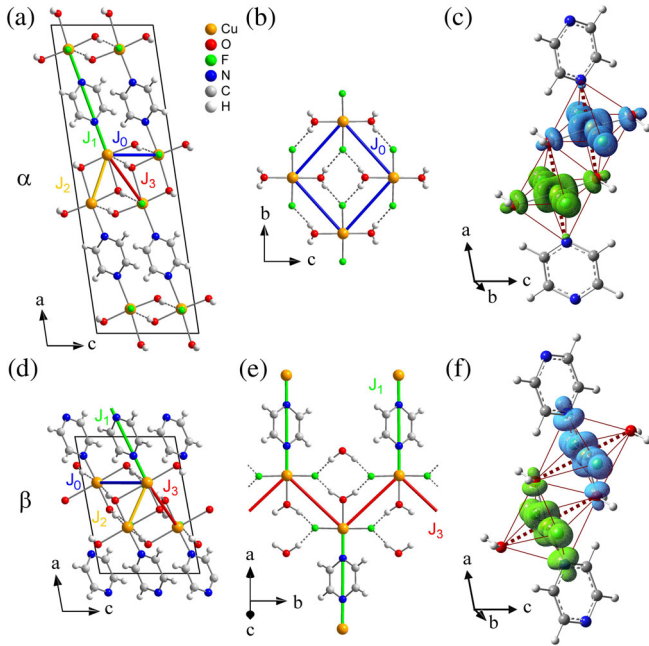


FIG. 3. Crystallographic structure of  $[\text{CuF}_2(\text{H}_2\text{O})_2]_2\text{pyz}$  in the  $\alpha$  phase, showing (a) the  $ac$  and (b) the  $bc$  plane. The dominant exchange parameter  $J_0$  is mediated by  $\text{Cu-O-H}\cdots\text{F-Cu}$  superexchange paths. (c) Calculated spin-density distribution of the ground state, with spins up and down represented, in cyan and green. Red lines mark the coordination octahedron of the  $\text{Cu}^{2+}$  ions and thick dashed lines the pseudo-Jahn-Teller axis. Structure in the  $\beta$  phase, showing (d) the  $ac$  and (e) the  $ab$  plane. The dominant exchange parameter  $J_3$  is mediated by  $\text{Cu-O-H}\cdots\text{F-Cu}$  paths. (f) Spin-density distribution; both the pseudo-Jahn-Teller axis and the magnetic orbitals are reoriented at the phase transition.

developed from quantum Monte Carlo (QMC) simulations for the spin-1/2 Q2D AFM Heisenberg model [33], where  $b = 2.43$  is a nonuniversal constant and  $\rho_s = 0.183J_0$  is the spin stiffness. This equation is valid for  $0.001 \leq J_\perp/J_0 \leq 1$  and is obtained from a modified RPA (Sec. S5 of the SM [15]).

From the zero-temperature estimates provided by these equations, we obtain self-consistent values for  $J_0(P)$  and  $J_\perp(P)$  by computing  $\chi(B)$  at the temperatures of our measurements. We perform QMC simulations using the stochastic series expansion with generalized directed loop updates [34] as implemented in the ALPS open-source code [35] and detailed in Sec. S6 of the SM [15]. The results of Fig. 1(b) can be reproduced with quantitative accuracy at all fields and pressures by using a nearest-neighbor  $XXZ$  Hamiltonian on a simple cubic lattice, as illustrated in Fig. 1(d) for the data at  $P = 1.5$  kbar. The spin-flop transition means that the  $\text{SU}(2)$  spin symmetry is broken down to  $\text{U}(1)$ , and the measured  $B_{\text{sf}}$  value is obtained by setting  $\Delta J_0^z = J_0^z - J_0 = 0.09$  K, i.e., with a 1% easy-axis anisotropy in  $J_0$ .

We show our results for  $B_c(P)$  in Fig. 2(b) and for  $J_0(P)$  and  $J_\perp(P)$  in Fig. 2(d). Linear fits for the low-pressure  $\alpha$

phase yield  $J_0(P) = a_0 + b_0P$  with  $a_0 = 11.4(1)$  K and  $b_0 = -0.34(1)$  K/kbar and  $J_\perp(P) = a_\perp + b_\perp P$  with  $a_\perp = 0.33(1)$  K and  $b_\perp = -0.005(1)$  K/kbar. As we quantify below, such a large coefficient for  $J_0$  is quite extraordinary. In Fig. 2(c) we show the ratio  $T_N/B_c$  as a function of pressure. Mean-field arguments predict both  $T_N$  and  $B_c$  to be proportional to the sum of all interactions and hence their ratio to be constant. However, quantum fluctuations in low-dimensional systems suppress  $T_N$  (to zero in the 1D and 2D limits) but not  $B_c$ . Our results imply that the Q2D system becomes slightly more 3D (i.e.,  $J_\perp/J_0$  increases) with increasing pressure up to 18 kbar.

The discontinuous change at 18 kbar marks a transition to a different low-dimensional magnetic phase. We find (below) that it is caused by a structural phase transition to a high-pressure  $\beta$  phase. Here, the  $J_3$  exchange becomes dominant, defining a system of AFM spin-1/2 chains, while  $J_\perp$  now corresponds to the arithmetic mean of  $J_0$ ,  $J_1$ , and  $J_2$ . For this Q1D case one has  $g\mu_B B_c = 2J_3 + 4J_\perp$

$$J_\perp = T_N / \{4c \sqrt{\ln(lJ_3/T_N) + 0.5 \ln[\ln(lJ_3/T_N)]}\}, \quad (2)$$

where  $c = 0.233$  and  $l = 2.6$  [33]. Once again we constrain the interchain couplings by RPA arguments [15] and refine self-consistent values for  $J_3(P)$  and  $J_\perp(P)$  in the  $\beta$  phase by QMC simulations. Linear fits to the results shown in Fig. 2(d) yield  $J_3(P) = a_3 + b_3P$  with  $a_3 = 12.7(1)$  K and  $b_3 = -0.15(1)$  K/kbar and  $J_\perp(P) = a_\perp + b_\perp P$  with  $a_\perp = 1.6(5)$  K and  $b_\perp = 0.03(1)$  K/kbar; the coefficient of  $J_3(P)$  is again anomalously large.

To place these results in context and to justify our use of “extraordinary,” we stress that compressive effects on magnetic exchange are expected due to reduced orbital separations and altered bond angles. These effects are generally at the 1% level in inorganic materials and the 10% level in organic ones. By “giant pressure dependence” we refer to far larger effects. Because a structural phase transition may, rather obviously, cause dramatic changes, we focus on continuous processes. Unusually large (10%) pressure effects known in inorganic systems [36,37] rely on proximity to a  $90^\circ$  bonding geometry. On a scale where our “pressure factor” is 2, the most extreme values we have found in organic materials range from 1.4 to 1.67 [38–41]; we are not aware of any microscopic explanations for these results. Here, we demonstrate that our observations are explained by an unconventional mechanism where the spin density evolves continuously between two different atomic orbitals, rather than remaining in one orbital whose shape changes slightly.

To understand our results we have performed structural investigations by x-ray diffraction in order to benchmark first-principles calculations using spin-polarized DFT. As detailed in Sec. S4 of the SM [15], we made high-pressure single-crystal x-ray diffraction measurements at ambient temperature and powder measurements at 5 K. The unit-cell parameters and bond distances for different pressures are

reported in Tables S1 and S2 of the SM [15] and full structural details are provided as crystallographic information files (CIFs). As represented in Fig. 3,  $\text{Cu}^{2+}$  ions are linked by  $\text{OH}\cdots\text{F}$  hydrogen bonds to form distorted square-lattice layers in the  $bc$  plane.  $\text{H}_2\text{O}$  ligands further connect these into a bilayer and pyz molecules link the bilayers into a 3D coordination network. In the  $\alpha$  phase [Figs. 3(a)–3(c)], the asymmetry in Cu coordination between the intralayer  $\text{Cu}^{2+}\text{—Cu}^{2+}$  bonds and the interlayer  $\text{H}_2\text{O}\text{—Cu}$ –pyrazine direction is referred to as “pseudo-Jahn-Teller”. Upon compression, both axial ligand bonds are shortened progressively. Because of the stronger field of the pyz ligand, the decreasing length of the Cu—N bond (from 2.40 to 2.30 Å, Table S2) is expected to have a stronger effect on the metal stereochemistry, and indeed we will find that this decrease is responsible for the giant pressure dependence of  $J_0$ .

A structural phase transition was observed at 18 kbar. The high-pressure  $\beta$  phase, shown in Figs. 3(d)–3(f), is characterized by a dramatic reduction of the Cu—N bond to 2.1 Å and an even stronger rise in the intralayer Cu—O separation (Table S2). This structural rearrangement represents a switch of the pseudo-Jahn-Teller axis [Fig. 3(f)]. However, we note that the Cu—N distance remains longer than for regular pyrazine coordination (2.05 Å).

We use the lattice symmetry and approximate atomic positions at ambient pressure as input for geometry optimizations within periodic DFT calculations, which we perform using CRYSTAL14 [42] as outlined in Sec. S7 of the SM [15]. These reproduce all of the observed structural features, including their evolution with pressure. They demonstrate that the  $\beta$  phase is more stable than  $\alpha$  for pressures above 20 kbar. Thus, the DFT calculations provide quantitative agreement on the critical pressure for the structural transition.

To investigate magnetic exchange in  $[\text{CuF}_2(\text{H}_2\text{O})_2]_2\text{pyz}$ , we identify the four Cu—Cu pathways shown in Fig. 3. We obtain the exchange parameters from the energy differences between high- and low-spin states of dinuclear fragments, calculated using the GAUSSIAN09 package [43] with the procedure described in Ref. [44] and summarized in Sec. S7 of the SM [15]. We find that the  $\text{Cu}^{2+}$  ions have the highest spin densities, with the remaining fraction delocalized on the ligands. In the  $\alpha$  phase, the magnetic orbitals involve  $\text{F}^-$  and  $\text{H}_2\text{O}$  ligands [Fig. 3(c)] and the primary contribution to  $J_0$  is from superexchange via Cu—O—H $\cdots$ F—Cu paths, making Q2D magnetic layers that match the structural square lattice [Fig. 3(b) and Ref. [45]]. The other exchange paths, marked  $J_1$ ,  $J_2$ , and  $J_3$  in Fig. 3(a), are poorly directed relative to the magnetic orbital and are small.

The calculated magnetic exchange parameters are shown in Fig. 4. DFT calculations without explicit account of correlation effects cannot in general obtain exchange parameters with quantitative accuracy, but their qualitative

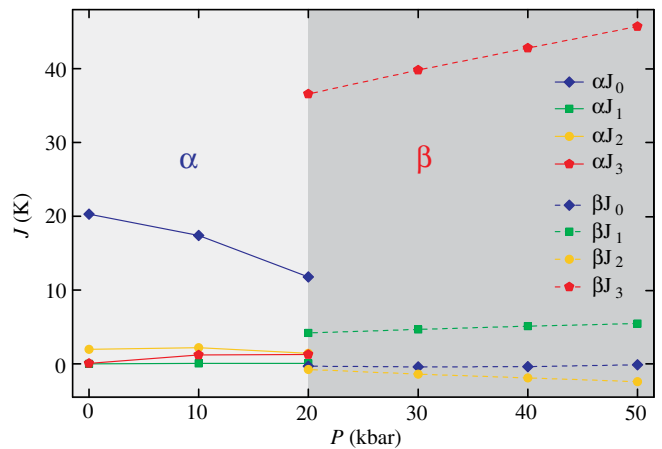


FIG. 4. Exchange parameters calculated as function of pressure for the  $\alpha$  and  $\beta$  phases using spin-polarized DFT.

features contain essential physical insight. Most importantly, the giant decrease of  $J_0$  in the  $\alpha$  phase is in good qualitative agreement with experiment [Fig. 2(d)]. Its microscopic origin lies primarily in the decrease of the axial Cu—N distance, which causes a systematic reduction of the equatorial spin density of the magnetic orbital [Fig. 3(c)]. DFT indicates further that all of the subdominant exchange parameters are small. Although this places them below the resolution limits of our calculations [46], it also supports the experimental analysis above. We draw attention to the trend visible in DFT that compression of the axial bonds enhances  $J_3$  strongly, from 60 mK at ambient pressure to 1.3 K at 20 kbar, without affecting  $J_1$  or  $J_2$  significantly.

In the  $\beta$  phase, the magnetic orbital revealed by the DFT spin density encompasses the two  $\text{F}^-$  ions and the (formerly axial) interlayer water and pyz ligands [Fig. 3(f)]. This orbital reorientation corresponds to the switch of the pseudo-Jahn-Teller axis and is responsible for the massive jumps in all of the exchange parameters (Fig. 4).  $J_3$  becomes dominant [Fig. 3(e)], while  $J_1$  is significantly smaller (by a factor of 9 in our calculations).  $J_0$  and  $J_2$  are weaker still, because they involve water ligands lying normal to the magnetic orbital [Fig. 3(f)], and hence the system becomes Q1D. This pressure-induced switching of orbital orientation and system dimensionality is analogous to the transitions reported for the “monolayer” material  $\text{CuF}_2(\text{H}_2\text{O})_2\text{pyz}$  [47,48] and occurs despite the less symmetric  $\text{Cu}^{2+}$  coordination of  $[\text{CuF}_2(\text{H}_2\text{O})_2]_2\text{pyz}$ . The monolayer system shows a relatively weak continuous pressure effect (1.17) [49] and no microscopic analysis of the magnetic interactions was provided.

Thus, our combined experimental and theoretical results both demonstrate unequivocally and explain qualitatively the dramatic changes in the magnetic properties of  $[\text{CuF}_2(\text{H}_2\text{O})_2]_2\text{pyz}$  under applied hydrostatic pressure. There are two quite different phenomena, namely (i) the giant but continuous decrease of the magnetic coupling

within the square lattice in the  $\alpha$  phase and (ii) a discontinuous switching of the dimensionality of magnetic exchange at 18 kbar. Our calculations show that the key structural feature explaining (i) is the compression of bonds along the pseudo-Jahn-Teller axis, which causes a progressive redistribution of spin density in the magnetic orbital driving a strong and systematic reduction of the in-plane exchange. (ii) is driven by an abrupt switch in orientation of this orbital, favoring the intrabilayer exchange path  $J_3$ , which establishes a Q1D magnetic network and explains the especially low  $T_N/B_c$  in Fig. 2(c).

While our first-principles structural calculations for  $[\text{CuF}_2(\text{H}_2\text{O})_2]_2\text{pyz}$  under pressure are reliable at a quantitative level, our spin-dependent energetic calculations are not. Nevertheless, they do reproduce correctly the order of importance and the ratios of the exchange parameters at all pressures on both sides of the transition [Figs. 4 and 2(d)]. One key qualitative point is the DFT insight into the hierarchy of exchange parameters, and specifically the fact that only one is dominant, which allows us to disentangle the subdominant ones by experiment from a formalism based only on parameters  $J_0$  or  $J_3$  and  $J_\perp$ . However, DFT does predict an increase of  $J_3$  with pressure in the  $\beta$  phase, in contrast to the decrease observed in experiment. We attribute this discrepancy to the limitations in our treatment of exchange correlations at the higher pressures. Finally, a particularly valuable feature of our DFT results is to show the relative contributions of the different ligands involved in the exchange processes, which is of vital importance in designing quantum magnets using metal-organic coordination polymers.

At a fundamental level, our experiments provide extreme sensitivity for investigating questions such as the evolution of entanglement in the many-body wave function, especially, close to quantum phase transitions. Neutron spectroscopy allows a direct probe of magnetic correlations and excitations. Recent measurements on  $\text{CuF}_2(\text{H}_2\text{O})_2\text{pyz}$  [50] revealed that the orbital reorientation induces a first-order transition of the magnetic excitations from spin waves to spinons. Our findings show that  $[\text{CuF}_2(\text{H}_2\text{O})_2]_2\text{pyz}$  is an even better candidate for such studies, not only because the key physics occurs at accessible pressure, field, and temperature conditions, but also because of the enormous range of parameter ratios spanned continuously by this material.

At a more applied level, our measurements make  $[\text{CuF}_2(\text{H}_2\text{O})_2]_2\text{pyz}$  an important model system for benchmarking any theoretical approach aiming to provide a quantitative description of magnetic properties from first principles. Our results afford direct insight into the toolkit of metal-organic chemistry, in terms of the ligands and linking units giving maximal flexibility and control of magnetic exchange. Thus, they provide an important step towards designing quantum magnets for applications in AFM spintronics, where we anticipate that pressure effects will be created using multiferroic substrate materials. For

such devices to be realized in layered heterostructures, it is critical that the dimensionality switching should leave the effective low-dimensional magnetic system in the plane of the layer, which is the case in  $[\text{CuF}_2(\text{H}_2\text{O})_2]_2\text{pyz}$  but not in  $\text{CuF}_2(\text{H}_2\text{O})_2\text{pyz}$ .

In summary, we have observed and explained a giant pressure dependence of the magnetic exchange in the metal-organic quantum magnet  $[\text{CuF}_2(\text{H}_2\text{O})_2]_2\text{pyz}$ . The combination of modern synthetic chemistry, high-precision physical measurements under extreme conditions, and state-of-the-art first-principles calculations allows essential calibration of theoretical methods and provides a promising strategy for designing quantum materials with tailored properties.

We thank R. Schwartz for professional engineering of the pressure cells and fixtures used for this study and acknowledge fruitful discussions with T. Giamarchi and N. Qureshi. Computations were performed at the Universities of Geneva and Bern on the Baobab and UBELIX clusters and using the resources of the Theory of Quantum Matter Group in Geneva. This research was supported by the EU FP7/2007-2013 under Grant No. 290605, the European Research Council (ERC) under the EU Horizon 2020 research and innovation programme Grant No. 681654, and the Swiss National Science Foundation (SNSF) under Grants No. 200020\_150257 and No. 200020\_162861, as well as through the SINERGIA Network ‘‘Mott Physics Beyond the Heisenberg Model.’’ J. G. was supported by an SNSF Early Postdoc Mobility fellowship during part of this work and M. S. by TRR80 of the German Research Foundation (DFG). We further acknowledge funding for measurements performed at the NHMFL by Grant No. DOE NNSA DE-NA0001979 with support by NSF Cooperative Agreement No. DMR-1157490 and the State of Florida.

---

\*bjorn.wehinger@unige.ch

†Present address: Microsoft Quantum, Redmond, Washington 98052, USA.

- [1] E. Dagotto and T. M. Rice, Surprises on the way from one- to two-dimensional quantum magnets: The ladder materials, *Science* **271**, 618 (1996).
- [2] B. Thielemann, Ch. Rüegg, H. M. Rønnow, A. M. Läuchli, J.-S. Caux, B. Normand, D. Biner, K. W. Krämer, H.-U. Güdel, J. Stahn, K. Habicht, K. Kiefer, M. Boehm, D. F. McMorrow, and J. Mesot, Direct Observation of Magnon Fractionalization in the Quantum Spin Ladder, *Phys. Rev. Lett.* **102**, 107204 (2009).
- [3] L. Savary and L. Balents, Quantum spin liquids: A review, *Rep. Prog. Phys.* **80**, 016502 (2017).
- [4] T. Jungwirth, X. Marti, P. Wadley, and J. Wunderlich, Antiferromagnetic spintronics, *Nat. Nanotechnol.* **11**, 231 (2016).
- [5] T. Kosub, M. Kopte, R. Hühne, P. Appel, B. Shields, P. Maletinsky, R. Hübner, M. O. Liedke, J. Fassbender, O. G.

- Schmidt, and D. Makarov, Purely antiferromagnetic magnetoelectric random access memory, *Nat. Commun.* **8**, 13985 (2017).
- [6] P. Wadley, B. Howells, J. Železný, C. Andrews, V. Hills, R. P. Campion, V. Novák, K. Olejník, F. Maccherozzi, S. S. Dhesi, S. Y. Martin, T. Wagner, J. Wunderlich, F. Freimuth, Y. Mokrousov, J. Kuneš, J. S. Chauhan, M. J. Grzybowski, A. W. Rushforth, K. W. Edmonds *et al.*, Electrical switching of an antiferromagnet, *Science* **351**, 587 (2016).
- [7] M. Conner, A. McConnell, J. Schlueter, and J. Manson, Structural and magnetic properties of copper(II) coordination polymers containing fluoride-based anions and ancillary organic ligands, *J. Low Temp. Phys.* **142**, 273 (2006).
- [8] P. A. Goddard, J. Singleton, P. Sengupta, R. D. McDonald, T. Lancaster, S. J. Blundell, F. L. Pratt, S. Cox, N. Harrison, J. L. Manson, H. I. Southerland, and J. A. Schlueter, Experimentally determining the exchange parameters of quasi-two-dimensional Heisenberg magnets, *New J. Phys.* **10**, 083025 (2008).
- [9] F. M. Woodward, P. J. Gibson, G. B. Jameson, C. P. Landee, M. M. Turnbull, and R. D. Willett, Two-dimensional Heisenberg antiferromagnets: Syntheses, x-ray structures, and magnetic behavior of  $[\text{Cu}(\text{pz})_2](\text{ClO}_4)_2$ ,  $[\text{Cu}(\text{pz})_2](\text{BF}_4)_2$ , and  $[\text{Cu}(\text{pz})_2(\text{NO}_3)](\text{PF}_6)$ , *Inorg. Chem.* **46**, 4256 (2007).
- [10] T. Lancaster, P. A. Goddard, S. J. Blundell, F. R. Foronda, S. Ghannadzadeh, J. S. Möller, P. J. Baker, F. L. Pratt, C. Baines, L. Huang, J. Wosnitza, R. D. McDonald, K. A. Modic, J. Singleton, C. V. Topping, T. A. W. Beale, F. Xiao, J. A. Schlueter, A. M. Barton, R. D. Cabrera *et al.*, Controlling Magnetic Order and Quantum Disorder in Molecule-Based Magnets, *Phys. Rev. Lett.* **112**, 207201 (2014).
- [11] P. A. Goddard, J. L. Manson, J. Singleton, I. Franke, T. Lancaster, A. J. Steele, S. J. Blundell, C. Baines, F. L. Pratt, R. D. McDonald, O. E. Ayala-Valenzuela, J. F. Corbey, H. I. Southerland, P. Sengupta, and J. A. Schlueter, Dimensionality Selection in a Molecule-Based Magnet, *Phys. Rev. Lett.* **108**, 077208 (2012).
- [12] P. A. Goddard, J. Singleton, C. Maitland, S. J. Blundell, T. Lancaster, P. J. Baker, R. D. McDonald, S. Cox, P. Sengupta, J. L. Manson, K. A. Funk, and J. A. Schlueter, Isotope effect in quasi-two-dimensional metal-organic antiferromagnets, *Phys. Rev. B* **78**, 052408 (2008).
- [13] J. L. Musfeldt, Z. Liu, S. Li, J. Kang, C. Lee, P. Jena, J. L. Manson, J. A. Schlueter, G. L. Carr, and M.-H. Whangbo, Pressure-induced local structure distortions in  $\text{Cu}(\text{pyz})\text{F}_2(\text{H}_2\text{O})_2$ , *Inorg. Chem.* **50**, 6347 (2011).
- [14] A. Lanza, C. Fiolka, M. Fisch, N. Casati, M. Skoulatos, C. Rüegg, K. W. Krämer, and P. Macchi, New magnetic frameworks of  $[(\text{CuF}_2(\text{H}_2\text{O})_2)_x(\text{pyz})]$ , *Chem. Commun.* **50**, 14504 (2014).
- [15] See the Supplemental Material at <http://link.aps.org/supplemental/10.1103/PhysRevLett.121.117201>, which contains Refs. [16-31].
- [16] C. T. Van Degrift, Tunnel diode oscillator for 0.001 ppm measurements at low temperatures, *Rev. Sci. Instrum.* **46**, 599 (1975).
- [17] W. A. Coniglio, L. E. Winter, C. Rea, K. Cho, and C. Agosta, Improvements to the tunnel diode oscillator technique for high frequencies and pulsed magnetic fields with digital acquisition, [arXiv:1003.5233](https://arxiv.org/abs/1003.5233).
- [18] S. Ghannadzadeh, M. Coak, I. Franke, P. A. Goddard, J. Singleton, and J. L. Manson, Measurement of magnetic susceptibility in pulsed magnetic fields using a proximity detector oscillator, *Rev. Sci. Instrum.* **82**, 113902 (2011).
- [19] D. E. Graf, R. L. Stillwell, K. M. Purcell, and S. W. Tozer, Nonmetallic gasket and miniature plastic turnbuckle diamond anvil cell for pulsed magnetic field studies at cryogenic temperatures, *High Press. Res.* **31**, 533 (2011).
- [20] K. Murata, K. Yokogawa, H. Yoshino, S. Klotz, P. Munsch, A. Irizawa, M. Nishiyama, K. Iizuka, T. Nanba, T. Okada, Y. Shiraga, and S. Aoyama, Pressure transmitting medium Daphne 7474 solidifying at 3.7 GPa at room temperature, *Rev. Sci. Instrum.* **79**, 085101 (2008).
- [21] J. Rodríguez-Carvajal, Recent advances in magnetic structure determination by neutron powder diffraction, *Physica (Amsterdam)* **192B**, 55 (1993).
- [22] CrysAlisPro 171.38.46 (2017).
- [23] G. M. Sheldrick, Crystal structure refinement with SHELXL, *Acta Crystallogr. Sect. C* **71**, 3 (2015).
- [24] P. R. Willmott, D. Meister, S. J. Leake, M. Lange, A. Bergamaschi, M. Böge, M. Calvi, C. Cancellieri, N. Casati, A. Cervellino, Q. Chen, C. David, U. Flechsig, F. Gozzo, B. Henrich, S. Jäggi-Spielmann, B. Jakob, I. Kalichava, P. Karvinen, J. Krempasky *et al.*, The Materials Science beamline upgrade at the Swiss Light Source, *J. Synchrotron Radiat.* **20**, 667 (2013).
- [25] S. Chakravarty, B. I. Halperin, and D. R. Nelson, Two-dimensional quantum Heisenberg antiferromagnet at low temperatures, *Phys. Rev. B* **39**, 2344 (1989).
- [26] A. D. Becke, Density-functional thermochemistry. III. The role of exact exchange, *J. Chem. Phys.* **98**, 5648 (1993).
- [27] C. Lee, W. Yang, and R. G. Parr, Development of the Colle-Salvetti correlation-energy formula into a functional of the electron density, *Phys. Rev. B* **37**, 785 (1988).
- [28] C. Gatti, V. R. Saunders, and C. Roetti, Crystal field effects on the topological properties of the electron density in molecular crystals: The case of urea, *J. Chem. Phys.* **101**, 10686 (1994).
- [29] E. Ruiz, J. Cano, S. Alvarez, and P. Alemany, Broken symmetry approach to calculation of exchange coupling constants for homobinuclear and heterobinuclear transition metal complexes, *J. Comput. Chem.* **20**, 1391 (1999).
- [30] J. Brambleby, J. L. Manson, P. A. Goddard, M. B. Stone, R. D. Johnson, P. Manuel, J. A. Villa, C. M. Brown, H. Lu, S. Chikara, V. Zapf, S. H. Lapidus, R. Scatena, P. Macchi, Y.-s. Chen, L.-C. Wu, and J. Singleton, Combining microscopic and macroscopic probes to untangle the single-ion anisotropy and exchange energies in an  $S = 1$  quantum antiferromagnet, *Phys. Rev. B* **95**, 134435 (2017).
- [31] Y. Zhao and D. G. Truhlar, The M06 suite of density functionals for main group thermochemistry, thermochemical kinetics, noncovalent interactions, excited states, and transition elements: Two new functionals and systematic testing of four M06-class functionals and 12 other functionals, *Theor. Chem. Acc.* **120**, 215 (2008).

- [32] D. J. Scalapino, Y. Imry, and P. Pincus, Generalized Ginzburg-Landau theory of pseudo-one-dimensional systems, *Phys. Rev. B* **11**, 2042 (1975).
- [33] C. Yasuda, S. Todo, K. Hukushima, F. Alet, M. Keller, M. Troyer, and H. Takayama, Néel Temperature of Quasi-Low-Dimensional Heisenberg Antiferromagnets, *Phys. Rev. Lett.* **94**, 217201 (2005).
- [34] F. Alet, S. Wessel, and M. Troyer, Generalized directed loop method for quantum Monte Carlo simulations, *Phys. Rev. E* **71**, 036706 (2005).
- [35] B. Bauer, L. D. Carr, H. G. Evertz, A. Feiguin, J. Freire, S. Fuchs, L. Gamper, J. Gukelberger, E. Gull, S. Guertler, A. Hehn, R. Igarashi, S. V. Isakov, D. Koop, P. N. Ma, P. Mates, H. Matsuo, O. Parcollet, G. Pawłowski, J. D. Picon *et al.*, The ALPS project release 2.0: open source software for strongly correlated systems, *J. Stat. Mech.* (2011) P05001.
- [36] M. Nishi, O. Fujita, J. Akimitsu, K. Kakurai, and Y. Fujii, High-pressure effects on the spin-Peierls compound  $\text{CuGeO}_3$ , *Phys. Rev. B* **52**, R6959 (1995).
- [37] P. Merchant, B. Normand, K. W. Krämer, M. Boehm, D. F. McMorrow, and Ch. Rüegg, Quantum and classical criticality in a dimerized quantum antiferromagnet, *Nat. Phys.* **10**, 373 (2014).
- [38] M. Mito, O. Fujita, M. Hitaka, T. Kawae, K. Takeda, S. Takagi, and H. Deguchi, Pressure effects of an  $S = 1$  Heisenberg antiferromagnetic bond alternating chain, *J. Phys. Soc. Jpn.* **70**, 1375 (2001).
- [39] M. Mito, H. Akama, H. Deguchi, S. Takagi, T. Kawae, K. Takeda, T. Ishii, M. Yamashita, H. Nakao, Y. Murakami, and S. Yamamoto, Pressure effects on an  $S = 1$  haldane compound  $\text{Ni}(\text{C}_5\text{H}_{14}\text{N}_2)_2\text{N}_3(\text{PF}_6)$ , *J. Phys. Soc. Jpn.* **72**, 399 (2003).
- [40] A. Sieber, D. Foguet-Albiol, O. Waldmann, S. T. Ochsenbein, G. Carver, H. Mutka, F. Fernandez-Alonso, M. Mezouar, H. P. Weber, G. Christou, and H. U. Güdel, Pressure dependence of the exchange interaction in the dimeric single-molecule magnet  $[\text{Mn}_4\text{O}_3\text{Cl}_4(\text{O}_2\text{CEt})_3(\text{py})_3]_2$  from inelastic neutron scattering, *Phys. Rev. B* **74**, 024405 (2006).
- [41] G. Seber, G. J. Halder, J. A. Schlueter, and P. M. Lahti, Pressure effects on the quasi-1-D molecular ferromagnet 2-(4,5,6,7-tetrafluorobenzimidazol-2-yl)-4,4,5,5-tetramethyl-4,5-dihydro-1H-imidazole-3-oxide-1-oxyl, *Cryst. Growth Des.* **11**, 4261 (2011).
- [42] R. Dovesi, V. R. Saunders, C. Roetti, R. Orlando, C. M. Zicovich-Wilson, F. Pascale, B. Civalleri, K. Doll, N. M. Harrison, I. J. Bush, P. D'Arco, M. Llunell, M. Causà, and Y. Noël, CRYSTAL14 User's Manual (unpublished).
- [43] M. J. Frisch, G. W. Trucks, H. B. Schlegel, G. E. Scuseria, M. A. Robb, J. R. Cheeseman, G. Scalmani, V. Barone, B. Mennucci, H. N. G. A. Petersson, M. Caricato, X. Li, H. P. Hratchian, A. F. Izmaylov, J. Bloino, G. Zheng, J. L. Sonnenberg, M. Hada, M. Ehara, K. Toyota *et al.*, GAUSSIAN 09 (Gaussian, Inc., Wallingford, CT, 2009).
- [44] L. H. R. Dos Santos, A. Lanza, A. M. Barton, J. Brambleby, W. J. A. Blackmore, P. A. Goddard, F. Xiao, R. C. Williams, T. Lancaster, F. L. Pratt, S. J. Blundell, J. Singleton, J. L. Manson, and P. Macchi, Experimental and theoretical electron density analysis of copper pyrazine nitrate quasi-low-dimensional quantum magnets, *J. Am. Chem. Soc.* **138**, 2280 (2016).
- [45] J. L. Manson, M. M. Conner, J. A. Schlueter, A. C. McConnell, H. I. Southerland, I. Malfant, T. Lancaster, S. J. Blundell, M. L. Brooks, F. L. Pratt, J. Singleton, R. D. McDonald, C. Lee, and M.-H. Whangbo, Experimental and theoretical characterization of the magnetic properties of  $\text{CuF}_2(\text{H}_2\text{O})_2(\text{pyz})$  ( $\text{pyz} = \text{pyrazine}$ ): A two-dimensional quantum magnet arising from supersuperexchange interactions through hydrogen bonded paths, *Chem. Mater.* **20**, 7408 (2008).
- [46] I. O. Thomas, S. J. Clark, and T. Lancaster, Exchange constants in molecule-based magnets derived from density functional methods, *Phys. Rev. B* **96**, 094403 (2017).
- [47] G. J. Halder, K. W. Chapman, J. A. Schlueter, and J. L. Manson, Pressure-induced sequential orbital reorientation in a magnetic framework material, *Angew. Chem., Int. Ed.* **50**, 419 (2011).
- [48] A. Prescimone, C. Morien, D. Allan, J. A. Schlueter, S. W. Tozer, J. L. Manson, S. Parsons, E. K. Brechin, and S. Hill, Pressure-driven orbital reorientations and coordination-sphere reconstructions in  $[\text{CuF}_2(\text{H}_2\text{O})_2\text{pyz}]$ , *Angew. Chem., Int. Ed.* **51**, 7490 (2012).
- [49] S. Ghannadzadeh, J. S. Möller, P. A. Goddard, T. Lancaster, F. Xiao, S. J. Blundell, A. Maisuradze, R. Khasanov, J. L. Manson, S. W. Tozer, D. Graf, and J. A. Schlueter, Evolution of magnetic interactions in a pressure-induced Jahn-Teller driven magnetic dimensionality switch, *Phys. Rev. B* **87**, 241102 (2013).
- [50] M. Skoulatos, M. Månsson, C. Fiolka, K. W. Krämer, J. Schefer, J. S. White, and Ch. Rüegg, Dimensional reduction by pressure in the magnetic framework material  $\text{CuF}_2(\text{D}_2\text{O})_2(\text{pyz})$ : From spin-wave to spinon excitations, *Phys. Rev. B* **96**, 020414 (2017).